Comparison of rolling contact fatigue damage between railway wheels and twin-disc test specimens

N.F. Strey, A.B. Rezende, R.S. Miranda, S.T. Fonseca, P.R. Mei, C. Scandian

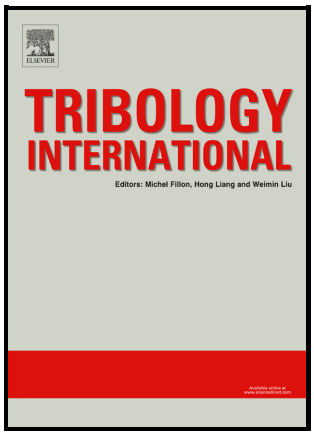

PII: S0301-679X(21)00185-7

DOI: https://doi.org/10.1016/j.triboint.2021.107037

Reference: JTRI107037

To appear in: *Tribiology International*

Received date: 14 December 2020
Revised date: 24 March 2021
Accepted date: 31 March 2021

Please cite this article as: N.F. Strey, A.B. Rezende, R.S. Miranda, S.T. Fonseca, P.R. Mei and C. Scandian, Comparison of rolling contact fatigue damage between railway wheels and twin-disc test specimens, *Tribiology International,* (2020) doi:https://doi.org/10.1016/j.triboint.2021.107037

Comparison of rolling contact fatigue damage between railway wheels and twin-disc test specimens

N. F. Strey[1], A. B. Rezende[2], R. S. Miranda[2], S. T. Fonseca[2], P. R. Mei[2], C. Scandian[1]*

[1]*Federal University of Espírito Santo, Department of Mechanical Engineering, 29075-910, Vitória, ES, Brazil.*

[2]*State University of Campinas, Faculty of Mechanical Engineering, 13083-860, Campinas, SP, Brazil.*

*Corresponding author: cherlio@hotmail.com

Abstract

Management of wheel-rail contact is of great importance for railways. It is essential to understand the tribology of railway materials to maximize productivity and reduce maintenance. Many studies on wear and rolling contact fatigue (RCF) were performed, ranging from field and full-scale experiments to small-scale tests, such as twin-disc. However, comparison between results found in these distinct approaches are few. Thus, RCF damage was compared between twin-disc specimens and wheels removed from field operation. Some aspects of RCF were remarkably similar, such as plastically deformed layer thickness, microhardness, crack angle and material delamination. However, cracks depth and length were 10 to 15 times larger in wheels. Finally, laboratory tests hardly simulate RCF in advanced stages and relevant environmental effects.

Keywords: rolling contact fatigue; steel; rail-wheel tribology; wear testing

1. Introduction

The ability to manage optimal conditions in the wheel-rail contact is of great importance for the operational efficiency of railways, as the nature of the contact induce a complex stresses state that is among the most severe of engineering applications [1, 2]. This is due to the interaction of several factors at the interface, such as: geometry of wheel and rail profiles [3], dynamic loads due to changes in the relief of the route and geometrical imperfections of the wheel and rail [4], increasingly high axle loads [5–8] and train speeds [9–11], manufacturing characteristics [12–14], and, chemical composition and microstructure of railway steels [15–20]. In addition, the wheel-rail contact is a classic example of an open tribosystem, where the presence of third bodies [20–26] and the influence of environmental conditions (temperature, humidity, contaminants) can be remarkable. Hence, the combined action of these tribological variables on the wheel-rail interface gives rise to different surface damage modes, such as rolling-sliding wear and rolling contact fatigue (RCF), resulting in premature failure of these components and threatening the safety of the entire railway system [1] [27,28].

The defect known as shelling consists of material loss due to the coalescence of surface or subsurface cracks that underwent nucleation and propagation by an RCF process [7, 29]. In wheels, the shelling damage starts at or below the tread, moving inward towards the rim core and, in extreme cases, can result in the vertical split rim fracture through a classic fatigue process guided by bending or impact loads [7, 30].

Robles Hernández et al. [14] found that metallurgical defects, such as pores and non-metallic inclusions, deteriorate the tensile and fatigue resistance of AAR Class C wheel steel, promoting the premature replacement of wheels due to excessive shelling. Moreover, Makino et al. [29] concluded that fatigue strength, as evaluated by shelling defect initiation, decreases with the increase of slip ratio.

Therefore, to maximize productivity and reduce maintenance costs, it is essential to understand the wheel-rail system, and how it is influenced by changes in contact conditions. In this sense, several methodologies of studies on wear and RCF have been performed, ranging from field experiments [31–34], to full scale test rigs [31, 35, 36] and small scale tests such as twin-disc [8, 9, 11, 13, 17, 19, 20].

Laboratory tests are used to simulate operating conditions on a small scale, to evaluate and characterize new materials, aiming cost reductions of railway operations [37]. Twin-disc is, perhaps, the best test option and has therefore been used extensively to test the fatigue and wear resistance of railway wheels and rails [38], because it allows the control and measurement of experimental variables [2], is economical and efficient when compared to other testing options [2, 39] and, is able to reproduce the pressure and slip conditions of the contact [40]. However, the approach with small scale tests may result in loss of information on the actual behavior of the materials, although there are correlations of wear and surface plastic deformation between laboratory and full scale tests [33].

Kráčalík et al. [39] reported that the contact area size in twin-disc tests is different from full scale tests. Thus, it may be incorrect to assume that the behavior of the material in the twin-disc test can be scaled to the real dimensions, since the contact and plastic deformation problems are non-linear. Lewis et al. [2] explained that the contact geometry in small scale tests is simplified, and that the conditions of the operating environment are difficult to be reproduced.

In contrast, Buckley-Johnstone et al. [36], performing dry and lubricated tests on a full scale rig and on twin-disc to evaluate the performance of a friction modifier, concluded that, in dry contact conditions, wear rates were statistically equal, while in the presence of the friction modifier the evolution of traction coefficient was similar in both tests. Lewis e Olofsson [34], while mapping wear coefficients for railway steels, gathered experimental data from field measurements and from twin-disc tests, and noted that the wear rate values reasonably agreed.

There are still many gaps in literature regarding the evaluation of similarities and differences, as well as the possibility of extending wear and RCF results found in laboratory tests to full scale tests and, ultimately, to actual railway conditions, which makes this type of work essential [2]. Therefore, to meet these needs, sought to compare the RCF damages, through morphological

and microstructural evaluation, observed on twin-disc test specimens and on wheels removed from field operation.

2. Materials and Methods

2.1 Materials

Steel wheels were removed from service in a heavy-haul railway, classified to transport 222 Mtkm of loads per year with speeds of up to 60 km/h. Two forged (initial hardness of 345 HBW, or 357 HV) and two cast (initial hardness of 332 HBW, or 345 HV) wheels presenting RCF-generated tread damage were selected at the field by visual inspection. These wheels were at the final of their lifespans, with rim thicknesses of 21-33 mm, measured at a distance of 80 mm from the back face of the rim. Another five wheels without visual tread damage were also selected for comparison. Table 1 shows the chemical composition of the steel and Figure 1a presents the typical microstructure, which is a very refined pearlite. During service, these wheels rolled over high strength fully pearlitic AREMA TR68 rails (0.8C-1.05Mn-0.25Si-0.25Cr), with yield limit of 890 MPa and surface hardness of 370 HBW (390 HV). Average roughness (Ra) of unused AREMA TR68 rails were 4.0 ± 0.3 µm (top of the rail), while on the defect free regions of the wheel treads removed from operation Ra = 5.6 ± 0.8 µm (using a 2.5 mm cut-off, according to ISO 4288:1996 [41]).

For twin-disc tests, the steel discs were removed from a new forged railway wheel. The chemical composition measured by optical spectrometry (ARL 3460 OES, Thermo Scientific) is also presented in Table 1. The upper discs were heat treated to ensure the pearlitic microstructure (Figure 1b). The specimens were austenitized at 900 °C, in a muffle furnace; then quick cooled (20 °C/s) to 600 °C and kept in a tin bath at 600 °C for 50 minutes, with subsequent air cooling.

Table 1 – Nominal chemical composition of the wheels removed from service (wt.%) [42], and chemical composition of the wheel steel used in the twin-disc test (wt.%).

Steel	C	Si	Mn	Cr	Cu	Mo+Nb
Wheel	0.67 - 0.77	0.15 – 1.00	0.60 – 0.90	< 0.25	< 0.35	-
Disc	0.71	0.43	0.84	0.27	0.21	0.22

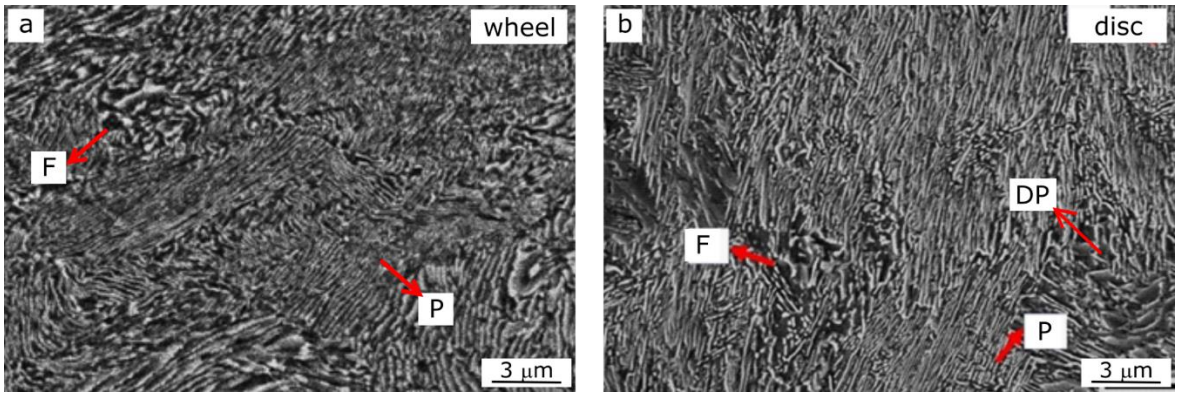

Figure 1 - (a) Typical very refined pearlitic microstructure of a forged wheel steel. (b) Initial microstructure of the pearlitic steel discs, 2% Nital. F – grain boundaries ferrite; DP – degenerated pearlite; P – pearlite.

2.2 Twin-disc tests

The tests were carried out in a twin-disc tribometer (Figure 2a), which simulates sliding-rolling contact fatigue [17]. Discs' thicknesses were 5 and 8 mm and they were positioned in the upper and lower axis, respectively (Figure 2b). Software monitors and controls the axes speeds and applied load, which promote an automatic operation of the tribometer. The slip effect was obtained from the angular speed difference between motor 1 and 2. The load was applied by a servo (motor 3) and a spindle system.

The discs positioned in the upper axis (called B) are the ones obtained from the heat treatment described earlier with 357 $HV_{0.5}$, while the discs positioned in the lower axis (called A) had a tempered martensite microstructure with 650 $HV_{0.5}$ of hardness using a steel with 0.68C-0.5Si-0.88Mn-0.13V chemical composition. This high hardness was used to minimize the plastic deformation and RCF damage in disc A, focusing the analysis only in the discs of pearlitic microstructure (disc B). Air jet removed debris from the disc interface and prevented excessive frictional heating of samples. Room temperature was from 25 °C to 30 °C and relative humidity ranged from 30 % to 60 %. The roughness (Ra) of the discs was measured by a portable contact-type surface roughness tester (SJ-210/Series 178, Mitutoyo) using ISO 4288:1996 standard [41] with cut-off length of 0.25 mm, along 10 sampling lengths. The initial surface roughness (Ra) was 0.20 µm ± 0.02 for all discs.

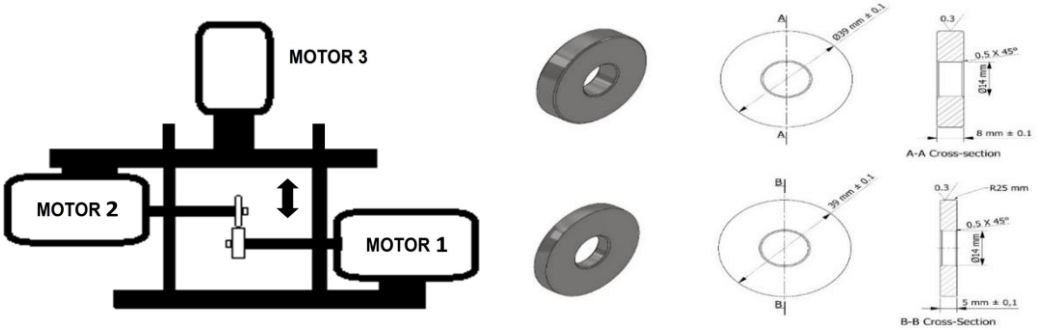

Figure 2 – (a) Schematic drawing of the twin-disc wear machine. (b) Dimension in millimeter of the discs used in the twin-tribometer.

Five replicas were performed for the twin-disc tests with the parameters described in

Table 2. For the sake of comparison, rotational speeds of actual wheels in service are up to 350 rpm, while slip ratios are typically 1% and up to 5%, depending on specific track conditions and wagon load. The initial (maximum) contact pressure was calculated by Hertz's theory [43–45] for non-conforming contact geometry. The tribometer constantly applied and controlled the load along the 100,000 cycles. The slip ratio was defined according to Zapata et al. and Fletcher and Beynon [46,47], as shown in Equation 1, where *N* is the rotational speed (rpm), *R* is the radius of the specimen (mm) and the subscripts indicate martensitic (A) and pearlitic (B) discs. Negative values of slip indicate that the disc B is driven by disc A. Disc B was installed in the lower speed axis to increment the tangential forces and accelerate the RCF damage in this disc.

$$Slip\ (\%) = 200 \times \left[\frac{(R_B \times N_B) - (R_A \times N_A)}{(R_B \times N_B) + (R_A \times N_A)}\right] \quad (1)$$

Table 2 – Parameters used on the twin-disc tribometer, according to AAR M-107/M208 [42].

Load	Initial (maximum) contact pressure	Slip ratio modulus	Total cycles	Axis rotation speed
2551 N	3150 MPa	0.75 %	100,000	Top (B) = 446.6 rpm Bottom (A) = 450.0 rpm

The characterizations were conducted in discs B, and the analyzed positions are illustrated in Figure 3. The discs were sectioned using an automatic precision cutting machine. Scanning electron microscopy (SEM) (EVO MA 15, Zeiss - UNICAMP) and optical microscopy (OM) (DMILM LED, LEICA - UNICAMP), were used: i) to analyze disc's surface (Figure 3a) and subsurface (Figure 3c); ii) for microstructural characterization (Figure 3c). Before twin-disc tests, Vickers microhardness was measured with a durometer (FV 800, Future Tech.), applying 0.5 kgf for 15 seconds in 12 circumferential positions (Figure 3b). After the tests, the Vickers microhardness profile was measured in a radial section (Figure 3c), beginning near the surface and towards the center, until hardness reached the bulk value, applying 0.3 kgf for 15 seconds.

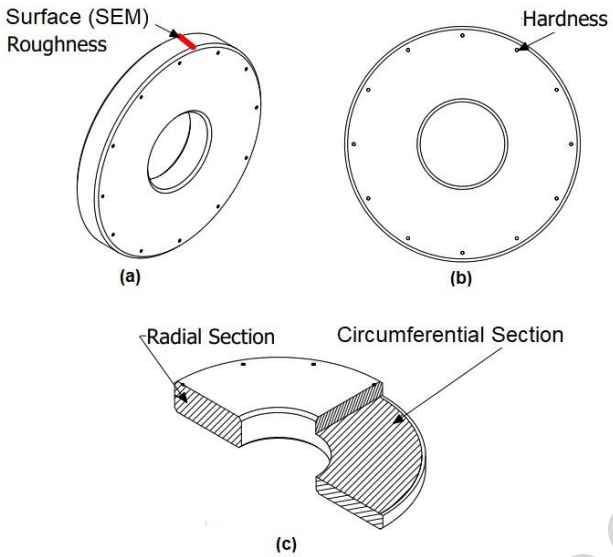

Figure 3 – Surface used for analysis: a) surface roughness, SEM; b) circumferential hardness on the face of the disc; c) radial section: hardness and SEM; circumferential section: OM and SEM.

2.3 Characterization of RCF damage on wheel treads after service

Rolling surfaces were evaluated by macro photography and SEM (JEOL JSM6010LA – USP), while metallographic analysis of radial and circumferential sections of wheels' rims (Figure 4), via OM (Nikon Eclipse MA200 - UFES) and SEM, revealed the subsurface microstructure. The wheels were sectioned using a horizontal band sawing machine and metalographic cutoff machine. Vickers (50 gf of load) and Brinell (187.5 kgf of load; 2.5 mm ball) tests through these sections mapped hardness at the micro and macro scale, respectively.

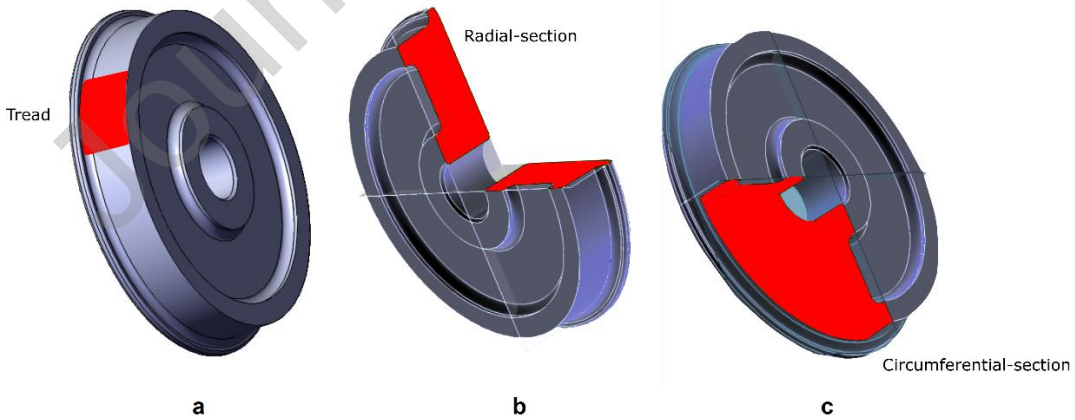

Figure 4 – Surfaces used for analysis of actual railway wheels: a) tread: macrophotography and SEM; b) radial section and c) circumferential section: hardness, OM and SEM.

3. Results and Discussions

3.1. Analyses of rolling surfaces of wheels and twin-disc specimens

Figure 5 presents a photograph of the radial section (refer to Figure 4b) of the wheel tread shown in Figure 6a (refer to Figure 4a), as well as its geometric profile, measured from image analysis via the software ImageJ1 [48]. The profile reveals that two depressions, caused by wear in two different rolling bands, generate a stress concentrator located in the center of the wheel tread and a false flange close to the chamfer. Therefore, it is no coincidence that shelling originated in the central region of the tread. The presence of the false flange may explain the microcracks observed near the chamfer of the wheel in Figure 6a, in addition to the lateral plastic flow of the tread that causes a protrusion of material at the rim chamfer. Thus, defects could be mitigated by improving the dynamics of the wagon truck, to distribute the surface wear more evenly along the tread, reducing the concentration of stresses and promoting the truncation of cracks generated by RCF.

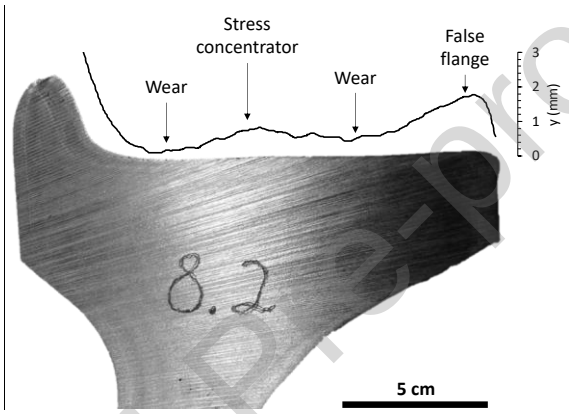

Figure 5 – Photograph of a radial section (Figure 6b) after sawing the wheel and tread profile obtained through image analysis. The region of the wheel tread where a geometric stress concentrator is observed corresponds to the region containing the shelling defect in this wheel.

Rolling surfaces of two moderately shelled wheels, one forged and one cast, are shown in Figure 6. Over almost the entire circumference and width of the surfaces, a characteristic metallic luster predominates, which suggests the continuous exposure of new surfaces by wear. Shelling, on both wheels, appears in the central region of the tread along much of the circumference, with greater severity in the cast wheel (Figure 6a) than in the forged wheel (Figure 6c), in this particular case. Shelling fracture surfaces are shown in greater magnification in Figure 6b and Figure 6d, for the cast and forged wheels, respectively. They are corroded and surrounded by a network of very fine surface microcracks, almost imperceptible to the naked eye, which are perpendicular to the direction of rolling. Microcracks of greater superficial extension and inclined in relation to the rolling direction, associated with shelling in its incipient stage (i.e., tread cracking), can be seen near the chamfer (at the field side of the rim) on the forged wheel (Figure 6e).

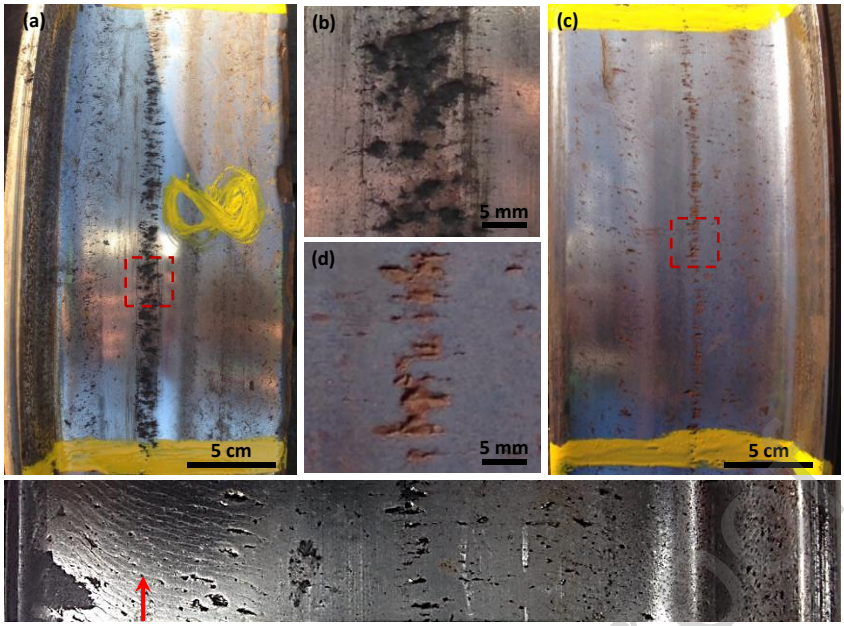

Figure 6 – Macroscopic aspect of shelling defect on wheel's tread after service. (a) Cast wheel, flange on the left. (b) Magnification of the region demarcated in (a). (c) Forged wheel, flange on the right. (d) Magnification of the region demarcated in (c). (e) Magnification of the entire length of the wheel tread shown in (c), arrow indicate rolling direction for both wheels.

Figure 7 presents the integrity of a disc's rolling surface after 100,000 cycles. The delamination present in the disc surface is similar to those identified in the Figure 6e (indicated by red arrow). The micrography (Figure 7b) showed several marks in the disc surface, and the dark areas may be delamination or removed particles. These superficial characteristics were also found in twin-disc tests with slip ratio of 20% [49].

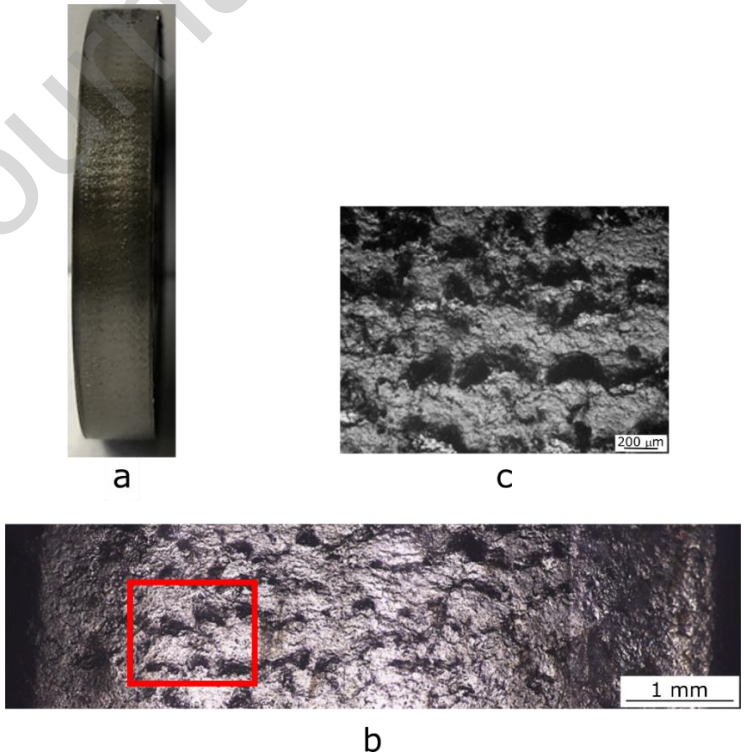

Figure 7 – Macroscopic aspect of shelling defect on discs after 100,000 cycles. (a) Discs tread (b) Magnification of the region in OM. (c) Magnification of the region demarcated in (b).

SEM images of wheel's and disc's surfaces (Figure 8) reveal that there are networks of RCF cracks. Both the actual wheel and the disc specimens were submitted to high magnitude cyclic stresses under unlubricated rolling-sliding conditions and there is direct evidence for the presence of surface and subsurface cracks, as well as microstructural distortion and strain-hardening of a heavily plastically deformed layer, as will be seen in the following sections, indicating that ratcheting is the main deterioration mechanism in both cases. This regime is characterized by the accumulation of plastic deformation at each cycle that results in depletion of the material's deformation capacity and, consequently, nucleation of superficial fatigue cracks [37,50]. A subsequent delamination process results in material detachment (i.e., wear) when the crack trajectory met the surface again [10,51–53]. Additionally, in wheels (Figure 8a), the red arrows indicate the presence of oxidation products located in crack's mouths, while, in disc specimens, there was no such evidence of oxidation.

The superficial analyses showed that the RCF defects found in the wheel removed from service and in the specimens from twin-disc tests are remarkably similar. This similarity of failure mechanisms indicates that these laboratory tests represent a good approximation of the surface integrity to be founded in the real scale wheel tread. A caveat should be made to environmental effects, such as oxidation, that may play a role in crack initiation and propagation but were not able to be fully reproduced in laboratory conditions.

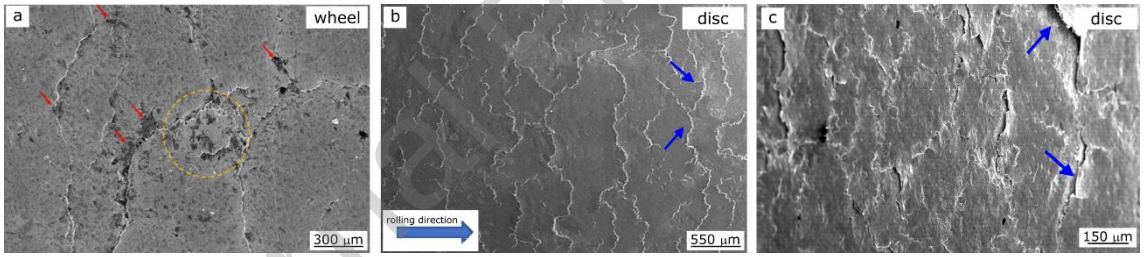

Figure 8 – (a) SEM micrograph of the tread surface of a forged wheel, showing the pattern of cracks (tread checks). The region demarcated by the circle comprises a particle, on the verge of detaching itself from the surface. The arrows indicate dark regions, which correspond to oxide material that forms or deposits at the cracks' mouths. (b) SEM images of a disc's rolling surface after 100,000 cycles. (c) SEM image of the same sample in (b) with a slightly tilted angle, highlighting delamination (blue arrows).

In the railway operation, eventually, contamination may occur in the contact between wheel tread and the top of rail by trace of lubricants [54]. According to Roy, Ooi and Sundararajan [55] for boundary lubrication regime micropitting commonly occur. This mechanism is drastically influenced by the relationship between the lubricant film thickness and surface roughness [56], [57]. Therefore, it was not ruled out the possibility of micropitting occurrence in the wheel tread illustrated in the Fig 8a. The micropitting is caused by RCF, manifesting as small cracks that nucleate and propagate on the surface, until a small portion of the material (in the order of a few μm) detaches [58], [59]. Comparing ratcheting and micropitting, both present a degree of morphological similarities, which makes them difficult to distinguish by analyzing only the surface micrographs. From the shakedown diagram, both mechanisms are product of surface fatigue [58], [54]. However, ratcheting act in plastic regime and is found in situation of severe

load, which promote incremental plastic deformation and fatigue of high cycle (conditions of this work). Micropitting takes place in the elastic shakedown regime and is characterized by high load and low friction coefficient (lubricated conditions) found mainly in cemented, nitrided, or carbon nitrided gear failures [55], [56], [60].

3.2. Evaluation of subsurface integrity in circumferential sections

Figure 9a shows a micrograph of the polished circumferential section of a forged wheel. A population of cracks is present. Virtually all of them culminate on the surface, suggesting that, likely, their genesis must be mostly superficial. For high loads and high friction coefficients (e.g., $\mu > 0.3$), the maximum principal shear stresses point is located at the surface of the rolling bodies. On the other hand, for lower friction coefficients, say $\mu < 0.2$, the point is located at the subsurface. These stresses are the ones responsible for the yield, strain-hardening and subsequent plastic depletion of the material during cyclic loading, resulting in microfracture by ratchetting. Therefore, surface induced cracks are predominant due to the high loads and expected high friction that is typical of unlubricated rolling contacts [61].

Each crack forms a shallow angle in its encounter with the surface, 14° to 20°, however, as it deepens in the material, the inclination progressively increases until the trajectory is perpendicular to the surface. At this point, some cracks branch into two propagation fronts: one that remains perpendicular and the other that tends to have smaller angles, or even are parallel to the surface (blue arrows). The intersection of a deeper parallel branch with an adjacent crack, which propagates perpendicular to the surface, can cause the removal of a large portion of material (shelling defect). However, the removal of small particles, through the intersection of cracks closer to the surface, is more frequent (white arrows). Figure 8a provides additional evidence to support this hypothesis, showing a small particle on the verge of detaching from the surface.

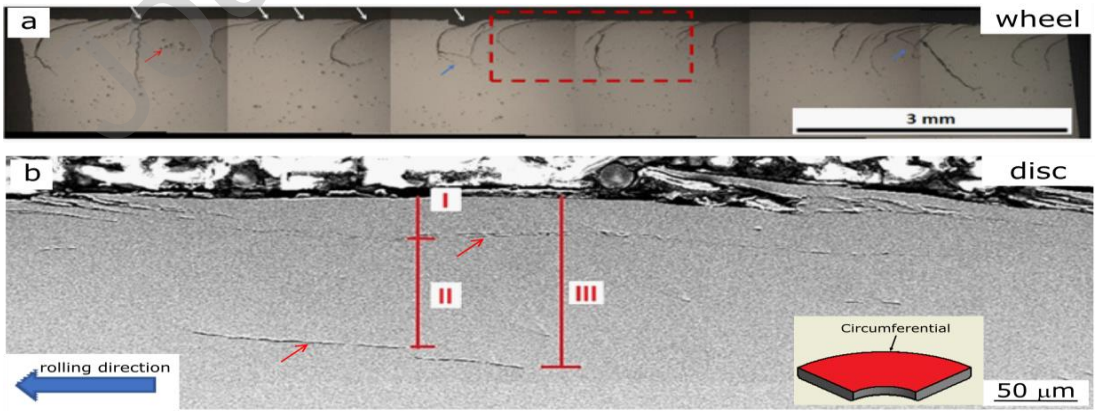

Figure 9 – (a) Optical micrograph of the polished circumferential section of a forged wheel tread after service. White arrows indicate regions where small particles have been removed, while blue ones point to intersections of cracks in the subsurface. (b) Scanning electron micrograph of the polished circumferential section subsurface of the disc after 100,000 cycles. The red lines indicate the cracks distance to surface. I = 30 µm; II = 112 µm; III = 130 µm.

The maximum crack depth, evaluated in the circumferential section of wheel treads, lies in the ranges of 0.1-0.7 mm and 0.1-1.0 mm for cast and forged wheels, respectively. Due to the limited sampling, it is not possible to state that there is a significant difference in the crack depth observed in forged and cast wheels. However, the somewhat similar range of depths may be characteristic of the contact conditions found at the railway.

Figure 9b presents the circumferential section micrograph of a pearlitic disc specimen. Likewise that on the wheel analysis, the disc presented cracks that originated on the surface and propagate to the subsurface of the disc, which configured the delamination process [50, 51]. However, these cracks did not propagate to a great depth as in the wheel. The crack angles were between 10° and 12° and they were very close to that found in the forged wheel (Figure 9a). The values of crack angles were also similar to found in other laboratorial twin-disc tests with slip ratios close of 0.75% [62–64]. Thus, when correlating the cracks of the two analyzed conditions, it is possible to conclude that the twin-disc test simulates a first stage of the crack's formation process. Wheel presented cracks in a more advanced propagation stage, which was evidenced by the much deeper cracks.

Regarding the distinctions on the crack depths, we propose the following explanations. The effect that would increase the depth of the cracks is the water in the wheel/rail contact due to the operation in rainy days. According to Hardwick, Lewis and Stock [65] , the addition of water in the contact causes crack growth due to hydro-pressurization or borderline growth under CFF (crack face friction) controlled shear. In their work, the addition of water in a disc's interface at twin-disc tests increased the crack depth in 600% compared to dry tests. In twin-disc tests performed in the present study, this effect was not present because the condition of tests was dry.

Another effect concerns the speed. According to He et al. [10], when the train speed increase, there is a significant increment in the wheel's RCF cracks. During the train operation, the speed varies because the different routes. In straight sections of the railway there is an acceleration period and, before curves, a deceleration period. Nonetheless, in the twin-disc tests the speed was kept constant. These differences observed in speed evolution between the studied conditions, associated with low number of cycles of twin-disc tests would also explain the higher depth in the cracks for wheel.

Kráčalík et al. [39] compared, using finite element method, the stress and strain states generated in the contact area of twin-disc specimens and full-scale wheel-rail experiment under the same number of cycles and contact pressure, considering cases with and without the presence of cracks. The model considered the material with a mixed isotropic and non-linear kinematic cyclic hardening behavior. The simulations indicated that the vertical contact stresses and the accumulated equivalent plastic strain had nearly the same magnitude and shape in all cases. However, the scale in the twin-disc case was smaller. Moreover, cracks deeper than 200 μm in the twin-disc model were located outside the region of higher magnitude stresses, i.e., they had no driving force to continue their propagation. On the other hand, in the wheel-rail

model, a crack of 1 mm was completely inside the zone with higher stresses, where a greater driving force is available to continue its growth. These numerical results corroborate the behavior shown in this work, where there were higher values of crack depth found in the actual wheels in relation to the cracks observed in the twin-disc laboratory tests.

The micrograph of Figure 9a still reveals that the metallurgical cleaning of the steel is not good, with levels of heterogeneities (non-metallic inclusions plus micro-porosities, indicated by the red arrow) around 1.0%, well above the 0.1% recommended by the AAR M-107/M-208 specification [42], although, in some cases, the assessed region has not coincided with that required by the standard. Similar levels were found for all evaluated wheels, whether forged or cast. Small deviations in the trajectory seem to cause the crack tip to meet these heterogeneities in the material, as they represent local stress concentrators. This inadequate metallurgical cleaning was also found in the twin-disc specimens (Figure 9b). Inclusions and voids, indicated by red arrows, were points of crack nucleation in the disc's subsurface. The cracks that begin in voids, inclusions, and sulfides (mainly MnS) propagate parallel and close to the contact surface and may accelerate the delamination, if the crack branch and coalesce up to the surface [66–68].

Figure 10a shows the microstructure of the circumferential section, showing that the crack appears in a plastically deformed layer on the surface, whose thickness is in the 127-250 µm range (95% confidence interval). The crack follows a trajectory that is tangent to the deformation lines until it finds the preserved microstructure at the aforementioned depth, which was subjected only to elastic stresses. As state before, the crack trajectory can either remain perpendicular to the surface, through the preserved microstructure, or is capable of branching, where its trajectory runs close to the interface between the plastically deformed layer and the non-deformed microstructure. Similar behavior is shown for the disc after 100,000 cycles in the Figure 10b. In the disc, there was a severe hardening in the surface, whose thickness varied in 255-270 µm range (95% confidence interval). The curvature of the deformed layers equally follows the rolling direction due to the tangential forces promoted by the contact load and the slip effect [49,69,70]. The thickness for both studied conditions was close, which proves the laboratorial test capacity to simulate some wheel damage characteristics.

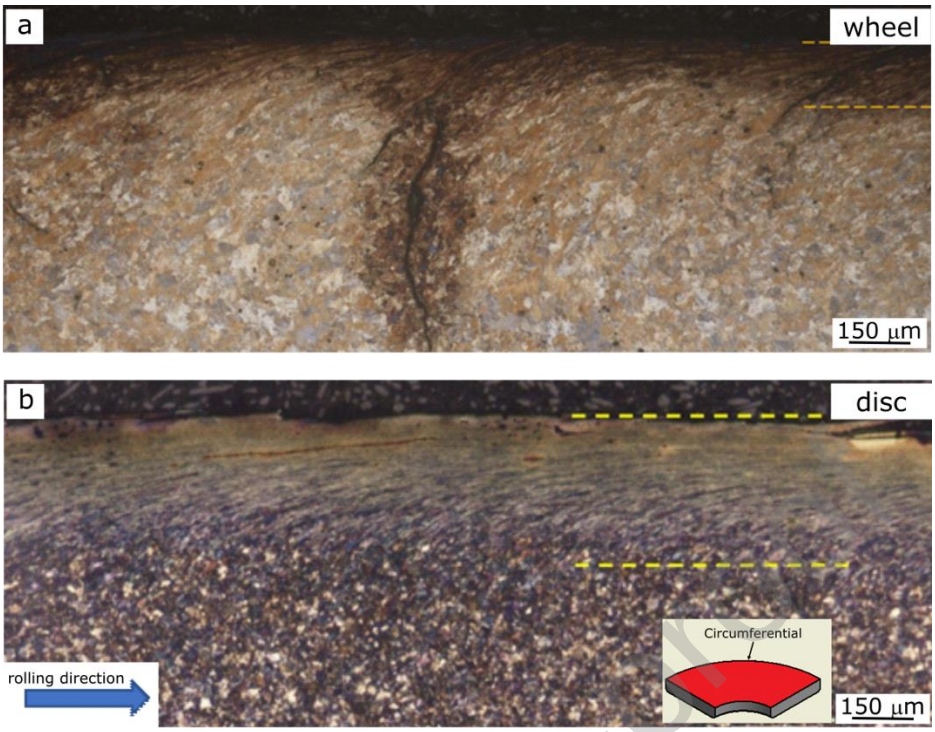

Figure 10 – (a) Magnification of the red box in Figure 9a (OM), circumferential section of a forged wheel tread after service (Nital 2% etchant). (b) Optical micrograph of the circumferential sectional view of the disc after 100,000 cycles (Nital 2% etchant).

The high deformation of the wheel steel pearlitic microstructure is shown in greater detail in Figure 11a-b, revealing that a significant in-service refinement took place near the rolling surface. The same effect is found in the disc subsurface after the twin-disc test (Figure 11c). The cementite lamellae align to the rolling direction, become thinner, more closely spaced, and also fractured [46,71]. There are very fine microcracks (indicated by red arrows) close to surface, where the deformation is more severe. These microcracks regularly propagate in the grain boundary ferrite and in the ferrite of the pearlite, which are aligned with the rolling direction [72,73]. The wide crack shown in Figure 11a is the one giving rise to the detachment of material (shell).

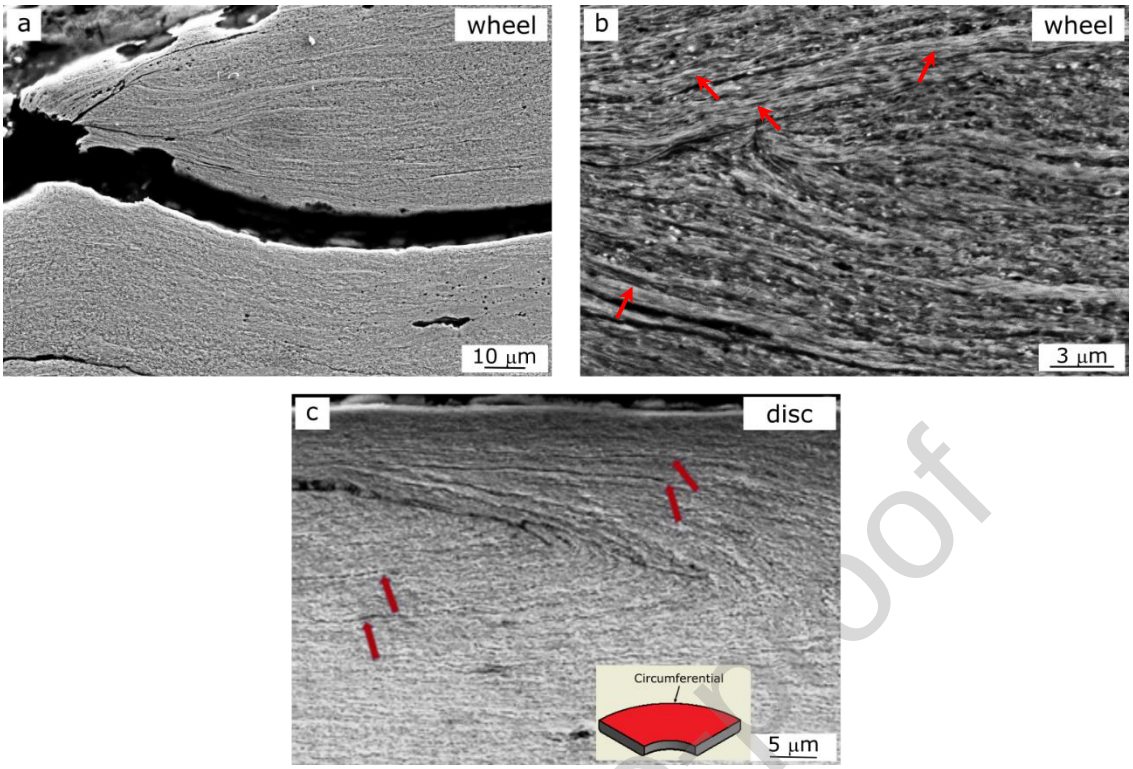

Figure 11. SEM of the radial section near the flange root of a cast wheel after service (2% Nital etching). (a) Region of the mouth of a superficial crack. (b) Magnification of the (a), showing great deformation of the microstructure and very fine microcracks running through the ferrite phase. (c) Scanning electron microscopy (SEM) image of the circumferential sectional view of the disc after 100,000 cycles (2% Nital etching). The red arrows indicate the microcracks.

3.3. Evaluation of subsurface integrity in radial sections

Figure 12a shows the radial section of the tread of the same wheel shown in Figure 9a. Subsurface cracks follow, parallel to the surface, with a much greater extension, from 5 to 15 mm, in the direction perpendicular to the rolling direction, which agrees with the superficial macroscopic observations (Figure 5). Portions of material at the surface can be observed without any connection with the material below them, which implies the imminence of shelling formation.

Figure 12b e Figure 12c illustrates the SEM images of the radial section of the pearlitic disc. Once again, there is a correlation between the twin-disc tests and the actual wheel. Figure 12b shows a crack that propagated parallel to the surface. The crack length is 850 µm and the depth is up to 31 µm. The crack illustrated in the Figure 12c has a smaller length of 500 µm and the depth of 20 µm. In the latter case, the propagation process was in an intermediate stage, since the crack begin closer the surface and propagates into the disc. This propagation behavior is similar to the one found in wheels (Figure 12a). From Figure 9 and Figure 12, it is possible to conclude that the crack propagation process is directionally-dependent, for both the disc and the wheel, and result in fracture surfaces typical of shelling defect (or delamination).

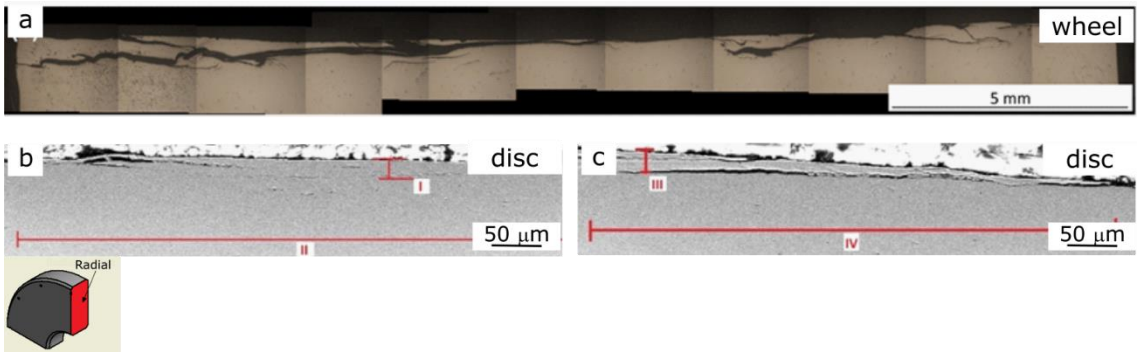

Figure 12 – (a) Optical micrograph of the polished radial section of a forged wheel tread after service. (b), (c) Scanning electron micrograph of polished radial sections disc specimens after 100,000 cycles. The red lines indicate cracks lengths or depths. I = 31 µm; II = 850 µm; III = 20 µm; IV = 500 µm.

The presence of water inside RCF cracks is common in railway's wheel-rail contact, due to rain or moisture. In its liquid state, water, when pressurized inside a crack by the rolling contact stresses, can accelerate its propagation through mode I loading (opening mode). Water and moisture present in the air are also able to corrode the faces of a crack originated from RCF, given the high susceptibility of carbon steel to corrosion. Figure 13 and Figure 8a corroborate this hypothesis, showing the presence of corrosion products inside cracks present on the wheel's rolling surface. Corrosion can affect fatigue processes, so also RCF, in different ways: i) cathodic or anodic reactions at the crack tip that accelerates crack propagation [74]; ii) wedging by corrosion products inside cracks can reduce the stress intensity amplitude (benefic effect), but increase its magnitude (malefic effect, [75]); iii) iron oxides have a relatively low shear resistance in sliding motion (compared to a metal-metal contact), promoting a lubricating effect between crack faces and, as a consequence, enabling mode II crack propagation (shear mode). For the tested conditions, twin-disc tests did not replicate the corrosive process occurring inside RCF cracks. This can be viewed as a limitation to the simulation of actual wheel-rail tribosystem's behavior, although many other important features are still present and give valuable information about it.

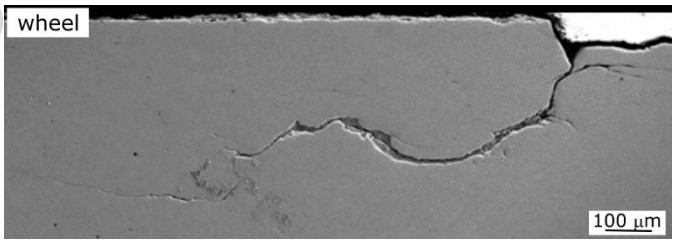

Figure 13 - SEM of the radial section at flange root of a cast AAR Class C wheel. Corrosion products accumulate inside the crack.

The considerable microstructural plastic deformation causes strain-hardening of a surface layer. The graph in Figure 14 shows microhardness profiles for wheels that showed shelling, or surface microcracks, and for wheels with "smooth" surfaces, i.e., without the presence of these defects, whether forged or cast. All wheels showed some level of hardening, presenting greater hardness close to the surface than in the bulk, which is 300-380 $HV_{0.05}$. However, surfaces that showed shelling or microcracks invariably strain-hardened more: microhardness at about 0.04

mm depth was in the range between 550 and 760 $HV_{0.05}$, while for smooth surfaces it was between 400 and 520 $HV_{0.05}$. Therefore, the higher hardness level of surfaces with microcracks or shelling indicates that the deformed layer has been plastically depleted, not supporting any increase in deformation without causing fracture, which is further evidence for ratcheting phenomenon. Depending on the evaluated depth, the microhardness threshold between ratcheted and “smooth” surface varies.

Figure 14 also shows evidence of strain-hardening on twin-disc test specimens. All hardness points for twin-disc tests specimens are inside of the hardness range found in wheels. At 0.03 mm depth the hardness was 570 $HV_{0,3}$ (hardness increment of 60%) and the value is in the range observed for shelled wheels at the same subsurface depth (Figure 14). Therefore, the twin-disc test is able to simulate the ratcheting mechanism caused by exhaustion of plasticity close to the surface. In both field and laboratory conditions, the farther from the surface the magnitude of contact stress are reduced, that results in less strain-hardening at greater depths. However, the strain-hardened layers of shelled wheels are much thicker than the ones of twin-disc test specimens, about 1 mm for the former versus 0.5 mm for the latter. The difference can be explained is terms of different residual elastic stress fields between the two, which is expected to be much greater in the wheels.

The effects of the contact stress in the subsurface can be divided in three regions [71]. Referring to Figure 10, in a first layer near the surface (delimitated by dashed lines) there is severe plastic deformation. Just below it, a transition region takes place, where elastic contact and residual stresses compete. Finally, a deeper region is characterized by contact stresses of negligible magnitude. The explanation correlates with the hardness profiles of Figure 14, where the disc initial hardness is only reached at a 0.5 mm depth, while the OM images reveals that the plastic deformed layer has a thickness of only 290 µm. The same is true for wheels, where some strain-hardening is observed up to 1 mm depth, while plastic deformed layer is only 255-270 µm thick.

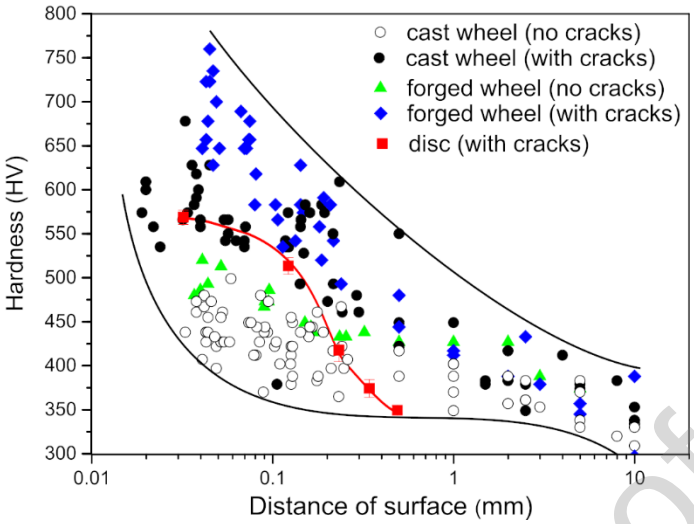

Figure 14 – Vickers microhardness profiles along the tread of the forged and cast wheel and hardness profile of the radial section of the disc ($HV_{0.3}$) (■). Surfaces that presented shelling or tread checking ($HV_{0.05}$) (● ◆) and a relatively smooth surface, i.e., without cracks ($HV_{0.05}$) (○ ▲).

Fracture surfaces, after the formation of a shelling defect in wheels, are quite irregular, as shown in Figure 15. Below it there is no plastically deformed material, which corroborates the observation of crack propagation parallel to the surface below the heavily strain-hardened layer. The defect edges become stress concentrating points and give rise to a new network of cracks that contribute to the material removal process, meaning that the defect increases in size by expanding its edges. This suggests that shelling progresses at an accelerated rate, since it is a feedback process: the greater the perimeter of the edge of the fracture surface, the more stress concentrating points are generated which, in turn, promote new material removal, expanding the perimeter of the edge, and so on. Understanding the edge effect can help determine the optimum timing for reprofiling of wheels, from economic and safety points of view.

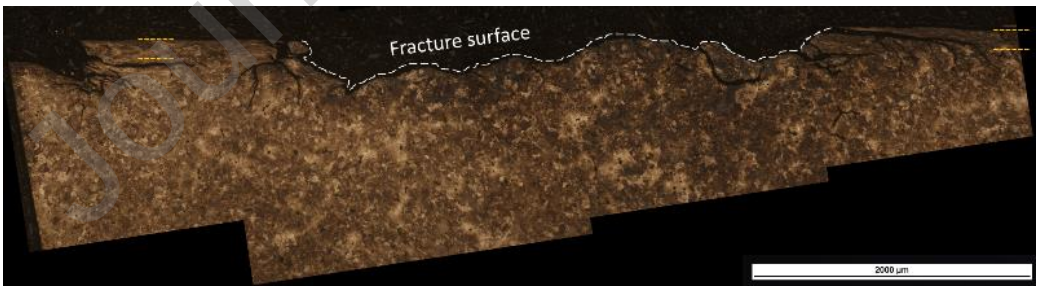

Figure 15. Optical micrograph of the circumferential section of the tread of a cast AAR Class C wheel (etched in Nital 2%). White dashes highlight the fracture surface of a shelling defect and yellow dashes denotes the plastically-deformed layer.

Wear was also observed in laboratory RCF tests. The wear coefficient determined by the Archard-Holm Equation [76] was $(4.6 \pm 0.1) \times 10^{-4}$ for the pearlitic disc (disc B). This value agrees with the one found by Ramalho et al. [77] after twin-disc tests with slip ratio close to 0.75% and is typical of a mild rolling-sliding wear regime, where plastic and oxidative processes play important roles [78]. Overall wear coefficients of wheel treads in railways are generally much lower than that. A rough estimation based on a wheel lifespan of 1.600.000 km, including material removal by reprofiling processes, is $k_{wheel} \sim 10^{-6}$. Closing the gap between

local (laboratory) and overall wear coefficients is not a trivial task, requiring the simulation of wheel profile evolution through computational algorithms, which is outside the scope of the present work.

A summary of the results is shown in Table 3. Some aspects of RCF damage were remarkably similar between wheels and discs, such as plastically deformed layer thickness, surface hardness and crack angle at mouth. Visual and SEM inspection of both rolling surfaces revealed a material delamination process caused by ratcheting. However, depth and length of cracks were 10 to 15 times larger in wheels than in discs, which correlates well with the difference in the diameter of contact area observed in each condition, ~ 11 mm and 1.7 mm, respectively. Moreover, the contact area lengths were in accordance with the values found by Zeng et al [79]. This indicates the influence of the stress field size on the difference between the depth and length cracks observed on the wheel and disc. Therefore, twin-disc test parameters suggest by AAR cannot simulate shelling defect in advanced stage, i.e., defects with large dimensions, for Class C wheel steel, but appears to be representative of the first stage of the defect formation, which is characterized by a ratcheting process. Finally, another marked difference between wheels and discs is the thickness of strain-hardened layer, twice larger for wheels due to the deeper elastic contact and residual stresses field.

Table 3 – Experimental results of the analysis of wheel and disc

Sample	Maximum RCF crack length (mm)	Maximum RCF crack depth (mm)	Crack angle at mouth (°)	Thickness of plastically deformed layer (μm)	Thickness of strain-hardened layer (mm)	Subsurface hardness at 0.04 mm depth (HV)
Wheel	15	1.0	14 - 20	127 - 250	~ 1.0	550 – 760 $HV_{0.05}$
Disc	0.85	0.13	10 - 12	255 - 270	~ 0.5	560 – 577 $HV_{0.3}$

4. Conclusions

Plastic stress and deformation fields are similar in wheels and twin-disc test specimens, considering their respective dimension proportion. The ratcheting process up to plastic exhaustion of a surface layer, followed by crack nucleation and its initial propagation inside the layer are very similar in both cases, meaning that affordable laboratory tests can give valuable information about the phenomena. However, when it comes to a more advanced crack propagation stage, deeply into the subsurface where only elastic stresses take place, twin-disc test fails to replicate conditions found in the actual railway wheels. The main reason for this is the contact area size difference between wheel-rail and twin-disc interfaces and the presence of contaminants (such as water, leaves, ores) in the wheel's operations.

The networks of cracks found at the edges of shelling craters in wheel treads suggest that the progression of the RCF damage in an advanced stage happens at an increasingly accelerated rate by the expansion of the crater's perimeter in a feedback process.

Corrosive processes and the influence of water that wheels face during service also were not replicated in AAR twin-disc test conditions. Water can pressurize crack tip and accelerate the propagation process. Moreover, it is well known that corrosive and fatigue processes act in synergy, accelerating damage in materials, specially steels. Evidence of corrosion products inside RCF cracks were found on wheels, but the extent of its effects on the damage mechanism is still not well stablished.

Acknowledgments

Funding: This work was supported by VALE S.A.

5. References

[1] A. Ekberg, B. Åkesson, E. Kabo, Wheel/rail rolling contact fatigue - Probe, predict, prevent, Wear. 314 (2014) 2–12. https://doi.org/10.1016/j.wear.2013.12.004.

[2] R. Lewis, E. Magel, W. Wang, U. Olofsson, S. Lewis, T. Slatter, A. Beagles, Towards a standard approach for the wear testing of wheel and rail materials, 231 (2017) 760–774. https://doi.org/10.1177/0954409717700531.

[3] R. Lewis, R.S. Dwyer-Joyce, S.R. Lewis, C. Hardwick, E.A. Gallardo-Hernandez, Tribology of the Wheel-Rail Contact : The Effect of Third Body Materials, Int. J. Railw. Technol. 1 (2012) 167–194. https://doi.org/10.4203/ijrt.1.1.8.

[4] A. Mazzù, L. Solazzi, M. Lancini, C. Petrogalli, A. Ghidini, M. Faccoli, An experimental procedure for surface damage assessment in railway wheel and rail steels, Wear. 342–343 (2015) 22–32. https://doi.org/10.1016/j.wear.2015.08.006.

[5] C. Qiu, J. Cookson, P. Mutton, The role of microstructure and its stability in performance of wheels in heavy haul service, J. Mod. Transp. 25 (2017) 261–267. https://doi.org/10.1007/s40534-017-0143-9.

[6] T. Reis, E. de A. Lima, F. Bertelli, A.A. dos Santos Junior, Progression of plastic strain on heavy-haul railway rail under random pure rolling and its influence on crack initiation, Adv. Eng. Softw. 124 (2018) 10–21. https://doi.org/10.1016/j.advengsoft.2018.07.003.

[7] D.J. Minicucci, S.T. Fonseca, R.L.V. Boas, H. Goldenstein, P.R. Mei, Development of niobium microalloyed steel for railway wheel with pearlitic bainitic microstructure, Mater. Res. 22 (2019) 8. https://doi.org/10.1590/1980-5373-mr-2019-0324.

[8] W. Solano-Alvarez, L. Fernandez Gonzalez, H.K.D.H. Bhadeshia, The effect of vanadium alloying on the wear resistance of pearlitic rails, Wear. 436–437 (2019) 203004. https://doi.org/https://doi.org/10.1016/j.wear.2019.203004.

[9] H.H. Ding, Z.K. Fu, W.J. Wang, J. Guo, Q.Y. Liu, M.H. Zhu, Investigation on the effect of rotational speed on rolling wear and damage behaviors of wheel / rail materials, 331 (2015) 563–570. https://doi.org/10.1016/j.wear.2014.12.043.

[10] C.G. He, J. Guo, Q.Y. Liu, W.J. Wang, Experimental investigation on the effect of operating speeds on wear and rolling contact fatigue damage of wheel materials, Wear. 364–365 (2016) 257–269. https://doi.org/10.1016/j.wear.2016.08.006.

[11] L. Rui, D. Liu, X. Zhao, C. Chen, An EBSD Investigation on the Evolution of the Surface Microstructure of D2 Wheel Steel During Rolling Contact Fatigue, Tribol. Lett. (2020) 1–11. https://doi.org/10.1007/s11249-020-1277-1.

[12] L.P.F. Almeida, L.E. Falqueto, H. Goldenstein, A.C. Bozzi, C. Scandian, Study of sliding wear of the wheel flange - Rail gauge corner contact conditions: Comparative between cast and forged steel wheel materials, Wear. 432–433 (2019) 102894. https://doi.org/10.1016/j.wear.2019.05.009.

[13] J.W. Seo, H.K. Jun, S.J. Kwon, D.H. Lee, Rolling contact fatigue and wear of two different rail steels under rolling-sliding contact, Int. J. Fatigue. 83 (2016) 184–194. https://doi.org/10.1016/j.ijfatigue.2015.10.012.

[14] F.C. Robles Hernández, S. Cummings, S. Kalay, D. Stone, Properties and microstructure of high performance wheels, Wear. 271 (2011) 374–381. https://doi.org/10.1016/j.wear.2010.10.017.

[15] A.B. Rezende, F.M. Fernandes, S.T. Fonseca, P.F.S. Farina, H.Goldenstein, P.R. Mei, Effect of alloy elements in time temperature transformation diagrams of railway wheels, Defect Diffus. Forum. 400 (2020) 11–20.

[16] S.T. Fonseca, A. Sinatora, A.J. Ramirez, D.J. Minicucci, C.R. Afonso, P.R. Mei, Effects of vanadium on the continuous cooling transformation of 0.7 %C steel for railway wheels, Defect Diffus. Forum. 367 (2016) 60–67. https://doi.org/10.4028/www.scientific.net/ddf.367.60.

[17] A.B. Rezende, S.T. Fonseca, F.M. Fernandes, R.S. Miranda, F.A.F. Grijalba, P.F.S. Farina, R. Mei, Wear behavior of bainitic and pearlitic microstructures from microalloyed railway wheel steel, Wear. 456–457 (2020) 203377. https://doi.org/10.1016/j.wear.2020.203377.

[18] A.P.A. Cunha, R.L. Villas Bôas, S.T. Fonseca, P.R. Mei, Effect of Microalloying on Structure and Properties of Hot Rolled 0.5 %C Steel, J. Metall. Eng. 2 (2013) 0–6.

[19] G. Zhang, C. Liu, R. Ren, S. Wu, H. Yin, X. Li, S. Wu, T. Cong, X. Li, Effect of nonuniform microstructure on wear property of ER8 wheel steel, Wear. 1 (2020). https://doi.org/10.1016/j.wear.2020.203416.

[20] A.B. Rezende, G.A. Amorim, D.J. Minicucci, S.T. Fonseca, P.R. Mei, Effect of vanadium addition on the surface roughness and fatigue crack propagation in a railroad wheel using twin disc wear test, Defect Diffus. Forum. 391 (2019) 66–73. https://doi.org/10.4028/www.scientific.net/ddf.391.66.

[21] L.E. Buckley-johnstone, G. Trummer, P. Voltr, A. Meierhofer, K. Six, D.I. Fletcher, R. Lewis, Tribology International Assessing the impact of small amounts of water and iron oxides on adhesion in the wheel / rail interface using High Pressure Torsion testing, Tribol. Int. 135 (2019) 55–64. https://doi.org/10.1016/j.triboint.2019.02.024.

[22] G. Trummer, L.E. Buckley-johnstone, P. Voltr, A. Meierhofer, R. Lewis, K. Six, Tribology International Wheel-rail creep force model for predicting water induced low adhesion phenomena, Tribiology Int. 109 (2017) 409–415. https://doi.org/10.1016/j.triboint.2016.12.056.

[23] W.A. Skipper, S. Nadimi, A. Chalisey, R. Lewis, Particle characterisation of rail sands for understanding tribological behaviour, Wear. 432–433 (2019) 202960. https://doi.org/10.1016/j.wear.2019.202960.

[24] K. Ishizaka, B. White, M. Watson, S.R. Lewis, R. Lewis, Influence of temperature on adhesion coefficient and bonding strength of leaf films : A twin disc study, Wear. 454–455 (2020) 203330. https://doi.org/10.1016/j.wear.2020.203330.

[25] S.R. Lewis, R. Lewis, G. Evans, L.E. Buckley-Johnstone, Assessment of railway curve lubricant performance using a twin-disc tester, Wear. 314 (2014) 205–212. https://doi.org/10.1016/j.wear.2013.11.033.

[26] S. Maya-Johnson, J. Felipe Santa, A. Toro, Dry and lubricated wear of rail steel under rolling contact fatigue - Wear mechanisms and crack growth, Wear. 380–381 (2017) 240–250. https://doi.org/10.1016/j.wear.2017.03.025.

[27] A. Bevan, P. Molyneux-Berry, B. Eickhoff, M. Burstow, Development and validation of a wheel wear and rolling contact fatigue damage model, Wear. 307 (2013) 100–111. https://doi.org/10.1016/j.wear.2013.08.004.

[28] B. Dirks, R. Enblom, M. Berg, Prediction of wheel profile wear and crack growth – comparisons with measurements, Wear. 366–367 (2016) 84–94. https://doi.org/10.1016/j.wear.2016.06.026.

[29] T. Makino, T. Kato, K. Hirakawa, The effect of slip ratio on the rolling contact fatigue property of railway wheel steel, Int. J. Fatigue. 36 (2012) 68–79. https://doi.org/10.1016/j.ijfatigue.2011.08.014.

[30] V. Sura, S. Mahadevan, Modeling of vertical split rim cracking in railroad wheels, Eng. Fail. Anal. 18 (2011) 1171–1183. https://doi.org/10.1016/j.engfailanal.2011.02.008.

[31] R. Stock, R. Pippan, RCF and wear in theory and practice-The influence of rail grade on wear and RCF, Wear. 271 (2011) 125–133. https://doi.org/10.1016/j.wear.2010.10.015.

[32] X. Gui, K. Wang, G. Gao, R.D.K. Misra, Z. Tan, B. Bai, Rolling contact fatigue of bainitic rail steels: The significance of microstructure, Mater. Sci. Eng. A. 657 (2016) 82–85. https://doi.org/10.1016/J.MSEA.2016.01.052.

[33] U. Olofsson, T. Telliskivi, Wear, plastic deformation and friction of two rail steels - A full-scale test and a laboratory study, Wear. 254 (2003) 80–93. https://doi.org/10.1016/S0043-1648(02)00291-0.

[34] R. Lewis, U. Olofsson, Mapping rail wear regimes and transitions, Wear. 257 (2004) 721–729. https://doi.org/10.1016/j.wear.2004.03.019.

[35] R. Stock, D.T. Eadie, D. Elvidge, K. Oldknow, Influencing rolling contact fatigue through top of rail friction modifier application - A full scale wheel-rail test rig study, Wear. 271 (2011) 134–142. https://doi.org/10.1016/j.wear.2010.10.006.

[36] L. Buckley-Johnstone, M. Harmon, R. Lewis, C. Hardwick, R. Stock, A comparison of friction modifier performance using two laboratory test scales, Proc. Inst. Mech. Eng. Part F J. Rail Rapid Transit. 233 (2018) 201–210. https://doi.org/10.1177/0954409718787045.

[37] R. Halama, R. Fajkoš, P. Matušek, P. Bábková, F. Fojtík, L. Václavek, Contact defects initiation in railroad wheels - Experience, experiments and modelling, Wear. 271 (2011) 174–185. https://doi.org/10.1016/j.wear.2010.10.053.

[38] E.A. Gallardo-Hernandez, R. Lewis, Twin disc assessment of wheel/rail adhesion, Wear. 265 (2008) 1309–1316. https://doi.org/10.1016/J.WEAR.2008.03.020.

[39] M. Kráčalík, G. Trummer, W. Daves, Application of 2D finite element analysis to compare cracking behaviour in twin-disc tests and full scale wheel/rail experiments, Wear. 346–347 (2016) 140–147. https://doi.org/10.1016/j.wear.2015.11.013.

[40] C. Kammerhofer, A. Hohenwarter, R. Pippan, A novel laboratory test rig for probing the sensitivity of rail steels to RCF and wear - first experimental results, Wear. 316 (2014) 101–108. https://doi.org/10.1016/j.wear.2014.04.008.

[41] ISO 4288:1996. Geometrical Product Specifications (GPS) - Surface texture: Profile method - Rules and procedures for the assessment of surface texture. ISO 4288. Geneva: International Organization for Standardization., (1996).

[42] “Association of American Railroad” AAR, Manual of standards and recommended practices, section G, M-107/M208, appendix C, topic 3.1.6, vol 1 (2011) 180 p.

[43] R. Galas, D. Smejkal, M. Omasta, M. Hartl, Twin-disc experimental device for study of adhesion in wheel-rail contact, Eng. Mech. 21 (2014) 329–334.

[44] W.R. Tyfour, J.H. Beynon, A. Kapoor, Deterioration of rolling contact fatigue life of pearlitic rail steel due to dry-wet rolling-sliding line contact, Wear. 197 (1996) 255–265. https://doi.org/10.1016/0043-1648(96)06978-5.

[45] R.L. Norton, Machine Design: an integrated approach, 4th Editio, 2010.

[46] D. Zapata, J. Jaramillo, A. Toro, Rolling contact and adhesive wear of bainitic and pearlitic steels in low load regime, Wear. 271 (2011) 393–399. https://doi.org/10.1016/j.wear.2010.10.009.

[47] D.I. Fletcher, J.H. Beynon, Equilibrium of crack growth and wear rates during unlubricated rolling-sliding contact of pearlitic rail steel, Proc. Inst. Mech. Eng. Part F J. Rail Rapid Transit. 214 (2000) 93–105. https://doi.org/10.1243/0954409001531360.

[48] C.A. Schneider, W.S. Rasband, K.W. Eliceiri, NIH Image to ImageJ: 25 years of image analysis, Nat. Methods. 9 (2012) 671–675. https://doi.org/10.1038/nmeth.2089.

[49] C. Hardwick, R. Lewis, D.T. Eadie, Wheel and rail wear—Understanding the effects of water and grease, Wear. 314 (2014) 198–204. https://doi.org/10.1016/J.WEAR.2013.11.020.

[50] Q. Li, X. Huang, W. Huang, Fatigue property and microstructure deformation behavior of multiphase microstructure in a medium-carbon bainite steel under rolling contact condition, Int. J. Fatigue. 125 (2019) 381–393. https://doi.org/10.1016/j.ijfatigue.2019.04.019.

[51] S.M. Hasan, D. Chakrabarti, S.B. Singh, Dry rolling/sliding wear behaviour of pearlitic rail and newly developed carbide-free bainitic rail steels, Wear. 408–409 (2018) 151–159. https://doi.org/10.1016/J.WEAR.2018.05.006.

[52] L. Ma, C.G. He, X.J. Zhao, J. Guo, Y. Zhu, W.J. Wang, Q.Y. Liu, X.S. Jin, Study on wear and rolling contact fatigue behaviors of wheel/rail materials under different slip ratio conditions, Wear. 366–367 (2016) 13–26. https://doi.org/10.1016/J.WEAR.2016.04.028.

[53] D. Zeng, L. Lu, N. Zhang, Y. Gong, J. Zhang, Effect of different strengthening methods on rolling/sliding wear of ferrite–pearlite steel, Wear. 358–359 (2016) 62–71. https://doi.org/10.1016/J.WEAR.2016.04.003.

[54] A. Mazzù, G. Donzella, A model for predicting plastic strain and surface cracks at steady-state wear and ratcheting regime, Wear. 400–401 (2018) 127–136. https://doi.org/10.1016/j.wear.2018.01.002.

[55] S. Roy, G.T.C. Ooi, S. Sundararajan, Effect of retained austenite on micropitting behavior of carburized AISI 8620 steel under boundary lubrication, Materialia. 3 (2018) 192–201. https://doi.org/10.1016/j.mtla.2018.08.029.

[56] T. Ahlroos, H. Ronkainen, A. Helle, R. Parikka, J. Virta, S. Varjus, Twin disc micropitting tests, Tribol. Int. 42 (2009) 1460–1466. https://doi.org/10.1016/j.triboint.2009.05.023.

[57] Y. Zhou, C. Zhu, B. Gould, N.G. Demas, H. Liu, A.C. Greco, The effect of contact severity on micropitting: Simulation and experiments, Tribol. Int. 138 (2019) 463–472. https://doi.org/10.1016/j.triboint.2019.06.020.

[58] P. Rycerz, A. Kadiric, The Influence of Slide–Roll Ratio on the Extent of Micropitting Damage in Rolling–Sliding Contacts Pertinent to Gear Applications, Tribol. Lett. 67 (2019) 1–20. https://doi.org/10.1007/s11249-019-1174-7.

[59] A. V. Olver, The mechanism of rolling contact fatigue: An update, Proc. Inst. Mech. Eng. Part J J. Eng. Tribol. 219 (2005) 313–330. https://doi.org/10.1243/135065005X9808.

[60] M.F. AL-Mayali, S. Hutt, K.J. Sharif, A. Clarke, H.P. Evans, Experimental and Numerical Study of Micropitting Initiation in Real Rough Surfaces in a Micro-elastohydrodynamic Lubrication Regime, Tribol. Lett. 66 (2018) 1–14. https://doi.org/10.1007/s11249-018-1110-2.

[61] J.A. Williams, The influence of repeated loading, residual stresses and shakedown on the behaviour of tribological contacts, Tribol. Int. 38 (2005) 786–797. https://doi.org/10.1016/j.triboint.2005.02.006.

[62] W.T. Zhu, L.C. Guo, L.B. Shi, Z.B. Cai, Q.L. Li, Q.Y. Liu, W.J. Wang, Wear and damage transitions of two kinds of wheel materials in the rolling-sliding contact, Wear. 398–399 (2018) 79–89. https://doi.org/10.1016/j.wear.2017.11.023.

[63] Y. Zhou, J.F. Peng, W.J. Wang, X.S. Jin, M.H. Zhu, Slippage effect on rolling contact wear and damage behavior of pearlitic steels, Wear. 362–363 (2016) 78–86. https://doi.org/10.1016/j.wear.2016.05.001.

[64] G. Donzella, A. Mazzù, C. Petrogalli, Competition between wear and rolling contact fatigue at the wheel—rail interface: some experimental evidence on rail steel, Proc. Inst. Mech. Eng. Part F J. Rail Rapid Transit. 223 (2009) 31–44. https://doi.org/10.1243/09544097JRRT161.

[65] C. Hardwick, R. Lewis, R. Stock, The effects of friction management materials on rail with pre existing rcf surface damage, Wear. 384–385 (2017) 50–60. https://doi.org/10.1016/j.wear.2017.04.016.

[66] A. Leiro, A. Kankanala, E. Vuorinen, B. Prakash, Tribological behaviour of carbide-free bainitic steel under dry rolling/sliding conditions, Wear. 273 (2011) 2–8. https://doi.org/10.1016/j.wear.2011.03.025.

[67] S.K. Dhua, A. Ray, S.K. Sen, M.S. Prasad, K.B. Mishra, S. Jha, Influence of nonmetallic inclusion characteristics on the mechanical properties of rail steel, J. Mater. Eng. Perform. 9 (2000) 700–709. https://doi.org/10.1361/105994900770345584.

[68] E.E. MAGEL, Rolling contact fatigue: a comprehensive review, 2011.

[69] M. Faccoli, A. Ghidini, C. Petrogalli, M. Faccoli, M. Lancini, A. Mazzù, Effect of desert sand on wear and rolling contact fatigue behavior of various railway wheel steels, Wear. 396–397 (2017) 146–161. https://doi.org/10.1016/j.wear.2017.05.012.

[70] B. Prakash, F.G. Caballero, R. Elvira, V. Smanio, T. Sourmail, C. Garcia-Mateo, K.G. Sundin, E. Vuorinen, A. Leiro, Wear of nano-structured carbide-free bainitic steels under dry rolling–sliding conditions, Wear. 298–299 (2012) 42–47. https://doi.org/10.1016/j.wear.2012.11.064.

[71] J.P. Liu, Y.Q. Li, Q.Y. Zhou, Y.H. Zhang, Y. Hu, L.B. Shi, W.J. Wang, F.S. Liu, S.B. Zhou, C.H. Tian, New insight into the dry rolling-sliding wear mechanism of carbide-free bainitic and pearlitic steel, Wear. 432–433 (2019) 202943. https://doi.org/10.1016/j.wear.2019.202943.

[72] Q.H. LI, C. ZHANG, H. CHEN, H. CHEN, Z. gang YANG, Microstructural evolution of a hypoeutectoid pearlite steel under rolling-sliding contact loading, J. Iron Steel Res. Int. 23 (2016) 1054–1060. https://doi.org/10.1016/S1006-706X(16)30157-1.

[73] C. Liu, R. Ren, D. Zhao, C. Chen, An EBSD investigation on the evolution of the surface microstructure of D2 wheel steel during rolling contact fatigue, Tribol. Lett. 68 (2020) 11. https://doi.org/10.1007/s11249-020-1277-1.

[74] T.L. Anderson, Fracture mechanics: fundamentals and applications, in: CRC Press, 2017.

[75] S.L. DEDMON, Effect of temperature on the performance of railway wheels. Proceedings of the Institution of Mechanical Engineers, J. Rail Rapid Transit. 231 (2017) 786–793.

[76] I.M. HUTCHINGS, Tribology Friction and Wear of Engineering Materials, Edward Arnold, Cambridge, 1992.

[77] A. Ramalho, Wear modelling in rail-wheel contact, Wear. 330–331 (2015) 524–532. https://doi.org/10.1016/j.wear.2015.01.067.

[78] P.J. Bolton, P. Clayton, Rolling—sliding wear damage in rail and tyre steels, Wear. 93 (1984) 145–165.

[79] D. Zeng, T. Xu, W. Liu, L. Lu, J. Zhang, Y. Gong, Investigation on rolling contact fatigue of railway wheel steel with surface defect, Wear. 446–447 (2020) 203207. https://doi.org/10.1016/j.wear.2020.203207.

CRediT authorship contribution statement

Nathan Fantecelle Strey: Conceptualization, Methodology, Validation, Investigation, Writing - Original Draft, Writing - Review & Editing. **Andrei Bavaresco Rezende:** Methodology, Validation, Investigation, Writing - Original Draft, Writing - Review & Editing. **Solange Tamara da Fonseca:** Methodology, Investigation, Writing - Original Draft, Writing - Review & Editing, Visualization. **Rodrigo S. Miranda:** Validation, Investigation, Writing - Original Draft, Writing - Review & Editing, Visualization. **Paulo Roberto Mei:** Conceptualization, Resources, Supervision, Funding acquisition. **Cherlio Scandian:** Conceptualization, Resources, Supervision, Project administration, Funding acquisition.

Declaration of interests

☒ The authors declare that they have no known competing financial interests or personal relationships that could have appeared to influence the work reported in this paper.

☐The authors declare the following financial interests/personal relationships which may be considered as potential competing interests:

Highlights

- Some aspects of RCF damage were remarkably similar between railway wheels and the twin-disc tests.
- Plastic stress and deformation fields were similar in wheels and twin-disc test specimens, considering their respective dimension proportion.
- The ratcheting process up to plastic exhaustion of a surface layer are very similar in both cases.
- Corrosive processes and the influence of water that wheels face during service were not replicated in AAR twin-disc test conditions.
- When it comes to a more advanced crack propagation stage twin-disc test fails to replicate conditions found in the actual railway wheels.